Materials Research Letters

ISSN: (Print) 2166-3831 (Online) Journal homepage: http://www.tandfonline.com/loi/tmrl20

Mechanically controlling the reversible phase transformation from zinc blende to wurtzite in AlN

Zhen Li, Satyesh Yadav, Youxing Chen, Nan Li, Xiang-Yang Liu, Jian Wang, Shixiong Zhang, Jon Kevin Baldwin, Amit Misra & Nathan Mara

To cite this article: Zhen Li, Satyesh Yadav, Youxing Chen, Nan Li, Xiang-Yang Liu, Jian Wang, Shixiong Zhang, Jon Kevin Baldwin, Amit Misra & Nathan Mara (2017) Mechanically controlling the reversible phase transformation from zinc blende to wurtzite in AlN, Materials Research Letters, 5:6, 426-432, DOI: 10.1080/21663831.2017.1303793

To link to this article: https://doi.org/10.1080/21663831.2017.1303793

MATER. RES. LETT., 2017
VOL. 5, NO. 6, 426–432
https://doi.org/10.1080/21663831.2017.1303793

MATERIALS RESEARCH LETTERS
Taylor & Francis
Taylor & Francis Group

ORIGINAL REPORT

Mechanically controlling the reversible phase transformation from zinc blende to wurtzite in AlN

Zhen Li[a,b], Satyesh Yadav[c], Youxing Chen[a], Nan Li[a,f], Xiang-Yang Liu[c], Jian Wang [d], Shixiong Zhang[b], Jon Kevin Baldwin[a], Amit Misra[e] and Nathan Mara[a,f]

[a]Center for Integrated Nanotechnologies, MPA-CINT, Los Alamos National Laboratory, Los Alamos, NM, USA; [b]Department of Physics, Indiana University, Bloomington, IN, USA; [c]Materials Science and Technology Division, MST-8, Los Alamos National Laboratory, Los Alamos, NM, USA; [d]Mechanical and Materials Engineering, University of Nebraska-Lincoln, Lincoln, NE, USA; [e]Department of Materials Science, University of Michigan, Ann Arbor, MI, USA; [f]Institute for Materials Science, Los Alamos National Laboratory, Los Alamos, NM, USA

ABSTRACT

III–V and other binary octet semiconductors often take two phase forms—wurtzite (wz) and zinc blende (zb) crystal structures—with distinct functional performance at room temperature. Here, taking AlN as a representative III–V compound, we investigate how to control the synthesized phase structure to either wz or zb phase by tuning the interfacial strain. By applying *in situ* mechanical tests at atomic scale in a transmission electron microscope, we observed the reversible phase transformation from zb to wz, and characterized the transition path—the collective glide of Shockley partials on every two {111} planes of the zb AlN.

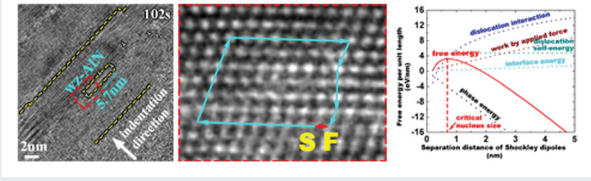

ARTICLE HISTORY
Received 7 November 2016

KEYWORDS
Reversible phase transformation; *in situ* TEM; aluminum nitride; wurtzite; zinc blende

IMPACT STATEMENT

The *innovation* of this paper is that a new type of plastic-deformation-driven reversible phase transition in AlN has been captured at atomic scale.

By virtue of the wide applications in nanoelectronics [1], quantum optics [2], and biological sensing [3], III–V and other binary octet semiconductor devices have recently attracted tremendous attention. Wurtzite (wz) and zinc blende (zb) are two common phases in these materials [4,5] and the crystal structure has been proven to be critical in determining the corresponding functional performance [2,6]. For example, by changing the crystal structure of GaP semiconductors from zinc blende to wurtzite, the band gap changes from indirect to direct, resulting in a significant enhancement of the efficiency of white light-emitting diodes [6]. Thus, controlling microstructure of the device made of such materials has motivated many experimental studies [6–12]. On the other hand, stress-induced phase transformation has been observed in these materials, via external stresses induced by heating [13], mechanical loading [14] or epitaxial burying [7]. However, such transformation is unidirectional.

As an important wide band-gap semiconductor [15], AlN is a widely investigated functional material. At ambient conditions, wurtzite is the most stable phase and the other two metastable phases possess zinc blende [16–18] and rock salt crystal structures. The phase transition from wurtzite to rock salt is only reported under shock loading [19–26], or extremely high pressure [20,26–29]. By virtue of lower phonon scattering, higher carrier mobility, better ferromagnetic properties, and enhanced light emission efficiency [30–33], many efforts have been devoted to stabilizing the metastable zinc blende phase in AlN

CONTACT Nan Li nanli@lanl.gov Center for Integrated Nanotechnologies, MPA-CINT, Los Alamos National Laboratory, Los Alamos, NM 87545, USA and Institute for Materials Science, Los Alamos National Laboratory, Los Alamos, NM 87545, USA; Jian Wang jianwang@unl.edu Mechanical and Materials Engineering, University of Nebraska-Lincoln, Lincoln, NE 68588, USA

Supplemental data for this article can be accessed here. https://doi.org/10.1080/21663831.2017.1303793

[34–36]. Nevertheless, understanding the mechanism and controlling the phase transformation between zinc blende and wurtzite are of pivotal importance, so that one can modulate the properties of AlN or prevent it from switching to undesired phases. Bimaterial interfaces, a common microstructural feature, can favor different phases by tailoring interfacial strain [37–39]. In this paper, we demonstrate the influence of interface strain on the phase transformation in AlN. Al/AlN nanoscale multilayers are used as a model structure.

The multilayered Al/AlN thin films were synthesized by reactive direct current magnetron sputtering (see Supplementary Methods). Figure 1(a) shows a cross-sectional transmission electron microscopy (TEM) image of the as-deposited film. The total film thickness is ~840 nm. The thickness of individual Al and AlN layers can be controlled by tuning the deposition time. The corresponding diffraction pattern, shown in Figure 1(b), indicates an Al {111} growth texture. The films have been divided into five zones with various individual volume ratio between Al and AlN. The microstructures of Zone 1 and Zone 2 are shown in Figure 1(c) and (d), respectively. In Zone 1, the average thickness of the AlN layers is 0.8 nm and that of the Al layers is 5.4 nm. In Zone 2, both layers are thicker: 3.9 nm for AlN and 12.3 nm for Al layers. The corresponding high-resolution TEM (HRTEM) images reveal the dependence of the phase structure of AlN on the layer thickness. As shown in Figure 1(c′), AlN exhibits zinc blende structure (labeled as zb-AlN afterwards) when the layer thickness is small. In Figure 1(d′), AlN has wurtzite structure (labeled as wz-AlN afterwards) in Zone 2 (see Supplementary Methods for a discussion of the structural difference between zb-AlN and wz-AlN and its implication in HRTEM images).

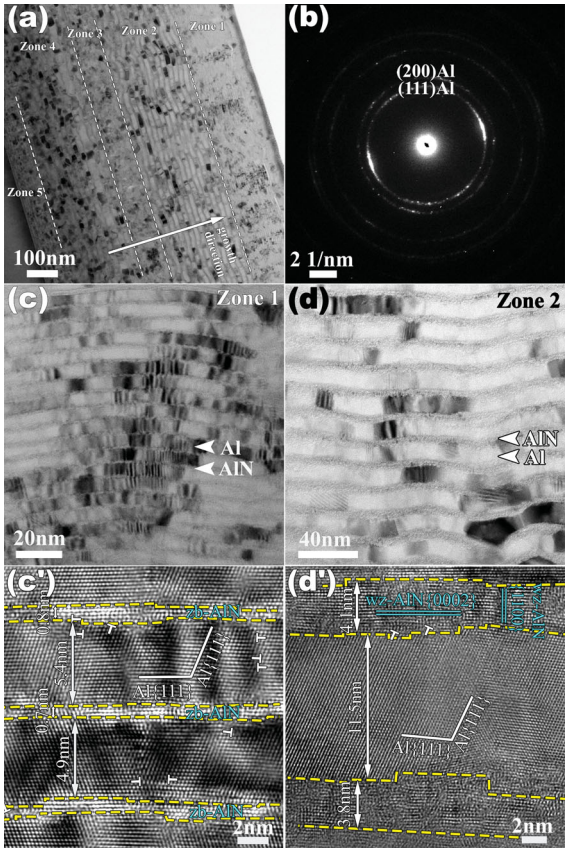

Figure 1. Investigation of AlN/Al multilayers by TEM. (a) A TEM image of the as-deposited film, in which five zones are categorized based on different morphologies, (b) the associated diffraction pattern, (c) and (d) magnified TEM images of Zone 1 and 2, respectively, and (c′) and (d′) HRTEM images in Zone 1 and 2 along the $<110>$ zone axis. The AlN phase structure and interface orientation relations have been identified: zb-AlN {111} || Al {111}, zb-AlN $<110>$ || Al $<110>$ in Zone 1, and wz-AlN (0002) || Al (-11-1), wz-AlN $<1120>$ || Al $<110>$ in Zone 2.

We performed *in situ* HRTEM indentation on the zb-AlN region to investigate the phase transformation mechanism in AlN. The schematic diagram of the *in situ* setup in a TEM is presented in the Supplementary. The compression direction is perpendicular to the interface plane and the displacement rate is controlled to be less than 1 nm/s. In Figure 2 and the movie in the Supplementary, the indenter is approaching the sample from the bottom right corner. During indentation testing, the phase structure of AlN evolves as recorded in the Supplementary Movie at a 15× accelerated speed. A series of HRTEM snapshots in Figure 2 reveal the phase transition in AlN under the indenter. As enclosed by the yellow dashed box in Figure 2(b), a finite volume of newly generated wz-AlN emerges in the middle of the original zb-AlN layer. The time of initiation of the phase transformation is arbitrarily defined as 0 s. The volume of the nucleated wurtzite phase grows as the indenter is further pushed into the film. This process is recorded from Figure 2(b)–(d) (from 0 to 102 s). Intriguingly, we found the reversible phase transformation when the local stress has been changed: the nucleated wz-AlN phase transforms back to zinc blende phase, and finally completely disappears (as shown in Figure 2(e) and (f)). As the phase transition progresses, the adjoining Al layers become thinner.

In addition to the equilibrium phase energy, the surrounding strain environments also play a significant role in determining the mechanism behind the transformation. Density functional theory (DFT)-based first-principles calculations are carried out to demonstrate the role of interface strain in triggering such a phase transition in AlN in Al/AlN multilayers. Computational supercells contain three layers (0.8 nm) and six layers (1.5 nm) of AlN (with either zb-AlN or wz-AlN phase, the schematics of which are presented in the Supplementary) and a varying number of Al layers.

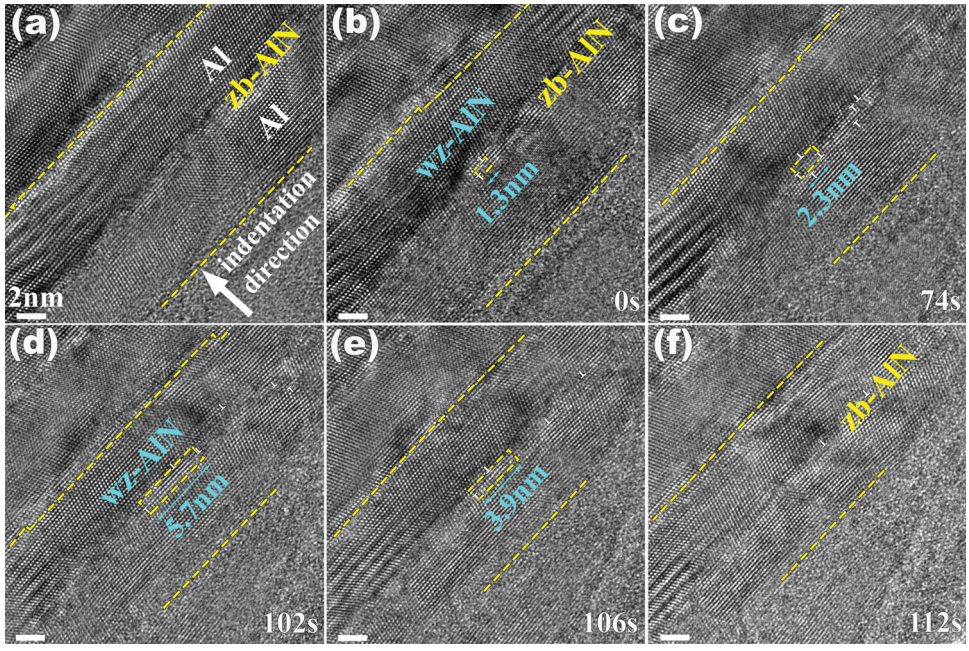

Figure 2. A series of HRTEM snapshots in the time order. (a) TEM image before phase transformation. The indenter is approaching the sample along the labeled direction, (b)–(d) a finite volume of newly generated wz-AlN presents in the middle of the AlN layer. The volume of the nucleated wurtzite phase grows as the indenter is pushed further into the film. The time of capturing the initiation of the phase transformation is arbitrarily defined as 0 s and (e)–(f) the nucleated wz-AlN phase transforms back to zinc blende upon continuously loading, and finally completely disappear.

During the energy minimization process, the computational supercell is allowed to change shape in all directions in order to release internal stresses associated with the phase transition (see Supplementary Methods for the DFT computational details). Because of the imposed coherent interface between Al layers and AlN layers, the interface remains a coherently strained state. It is found that for both three-layer and six-layer AlN cases, the relative cohesive energies of the supercell containing zb-AlN compared to that containing wz-AlN depend on the number of Al layers in the model, as shown in Figure 3. The magnitude of the relative energy ($E_{zb} - E_{wz}$) decreases as the number of Al layers increases. At ~ 32 Al layers (6.8 nm), the Al/AlN supercell containing three layers of AlN energetically prefers to form the zinc blende phase, rather than the wurtzite phase, which is indeed the case for the thin zb-AlN layers in Zone 1. The DFT results are further analyzed by partition of the relative cohesive energies into interface-related energy term and strain energies term. The energy related to interfaces (including interface energy and interface–interface interaction energy) is calculated to be $\sim -45\ \mathrm{mJ/m^2}$ ($E_{zb}^{int} - E_{wz}^{int}$) in the three-layer case and $-63\ \mathrm{mJ/m^2}$ ($E_{zb}^{int} - E_{wz}^{int}$) in the six-layer case, respectively, which suggests that the zb-AlN/Al interface has lower formation energy than the wz-AlN/Al interface. In addition, as the biaxial coherency strain at the interface increases, the energy

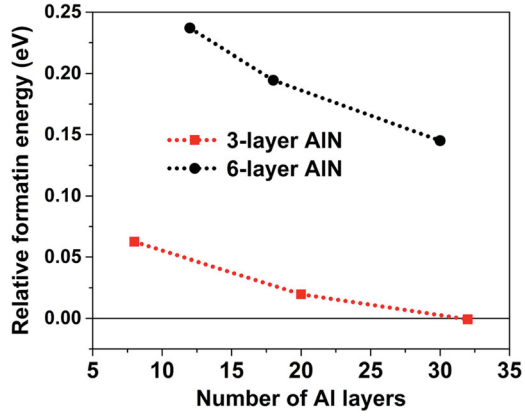

Figure 3. DFT calculations of the relative formation energy of Al/AlN with AlN in zinc blende phase compared to with AlN in wurtzite phase. Positive energy implies wz-AlN is more stable than zb-AlN.

difference between the zb-AlN/Al interface and the wz-AlN/Al interface also decreases because of the diminishing cohesive energy difference between bulk zb-AlN and bulk wz-AlN [40]. Thus, for thin AlN layers, the zb-AlN/Al interface is more thermodynamically stable than the wz-AlN/Al interface. As the layer thickness increases, wz-AlN will eventually form, as is the case in Zone 2 of the microstructure presented here.

The observed phase transformation from zinc blende to wurtzite in AlN (as shown in Figure 2) can be

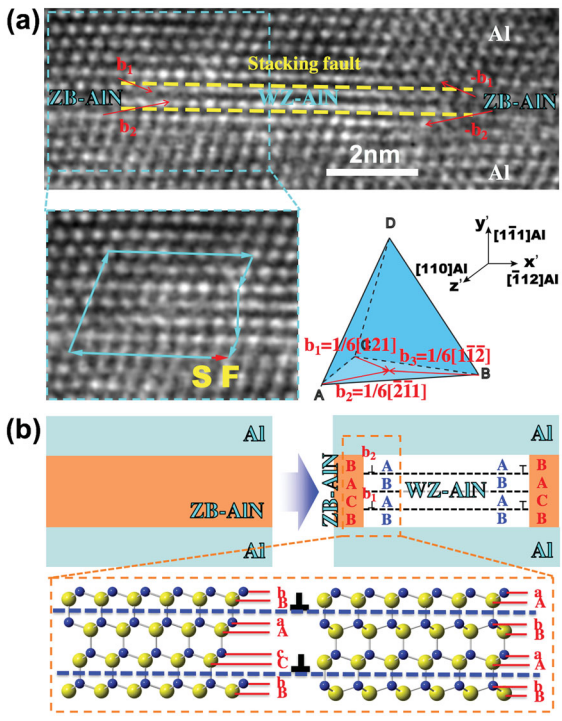

Figure 4. Phase transformation mechanism. (a) The magnified atomic configuration of newly generated new phase in Figure 2(d). Two stacking faults are identified by the yellow dashed lines. The Thompson tetrahedron shows all three Shockley partials on the {111} plane. The overall Burgers vector of the Shockley partials composing the left-hand side vertical phase boundary has been identified through the Burgers circuit, starting at 'S' and ends at 'F' and (b) the schematic diagram of the whole transition process is illustrated, and can be realized as the nucleation and extension of two Shockley dislocation dipoles.

treated as the nucleation and extension of Shockley partial dislocation dipoles on every two zb-AlN {111} planes [13,14]. Figure 4(a) shows the magnified atomic configuration of the newly generated wurtzite phase and a sharp vertical boundary with the pre-existing zb-AlN. The zb-AlN/Al interface is coherent, and along $<110>$ zone direction, the zb-AlN follows the same stacking sequence as the adjoining Al layers. However, across the region of the newly generated phase, two stacking faults can be identified (highlighted by yellow dashed lines). The microstructure of the left-hand side vertical phase boundary has been further magnified. Here the line direction of the nucleated partials is chosen to be pointing into the plane of the page, and the corresponding Burgers circuit, which starts at the symbol 'S' and ends at symbol 'F', is plotted to determine the overall Burgers vector. The sum of the two nucleated Shockley partials is $\frac{a_0}{6}[\bar{1}12]$. The Thompson tetrahedron in Figure 4(a) shows all three Shockley partials on the {111} plane. The creation of stacking faults can be realized through the glide of any of the Shockley partials. However, in order to reach the sum of $\frac{a_0}{6}[\bar{1}12]$, the two nucleated Shockley partial dislocations have to possess the same edge components with opposite screw components (labeled as $\mathbf{b_1}$ and $\mathbf{b_2}$ here). With opposite screw components between $\mathbf{b_1}$ and $\mathbf{b_2}$, the attractive interaction inhibits them from breaking apart, producing a sharp in-layer phase boundary. With the same edge components, they glide in a similar direction under an applied shear stress [41–43]. The reversibility of the observed phase transformation can be attributed to the glide of Shockley partials, $\mathbf{b_1}$ and $\mathbf{b_2}$, in the opposite direction, which in turn annihilates their negative components. The whole process has been illustrated in the Figure 4(b). Here the atomic planes with capital symbol (A, B or C) represent the compact atomic plane comprised of Al atoms and lower case (a, b, or c) comprised of N atoms.

The phase transformation from zb-AlN to wz-AlN observed in *in situ* indentation tests is driven by the accumulated compressive strain energy in the sample. In the as-deposited state, the in-plane compressive interface strain stabilizes the zb-AlN phase over the wz-AlN phase. When an external compressive strain is applied normal to the interface, the difference in cohesive energy between zb-AlN and wz-AlN increases, which will make the high energy phase increasingly unstable [40]. Release of the strain energy stored in AlN can be accomplished via two pathways: (i) plastic deformation developed in Al layers and (ii) phase transformation occurring in the zinc blende phase. These may not happen simultaneously, but are influenced by one another. In the Al layer, development of plastic deformation is through nucleation and propagation of lattice dislocations from the adjoining Al/AlN interfaces, resulting in thinning of the Al layer. This has been captured in our *in situ* observations. In the AlN layer, phase transformation between wurtzite and zinc blende is accomplished through nucleation and glide of Shockley partial dislocations [41–43]. From an energetic viewpoint, such a transformation must overcome an energy barrier under applied stress, which corresponds to the nucleation of Shockley partial dipoles in the zinc blende phase. Since the Burgers vector of the nucleated dislocations is known, the interaction energy and dislocation self-energy can be estimated from linear elastic dislocation theory [44]. The differences in the interface and cohesive energies between zb-AlN and wz-AlN are obtained from the current DFT studies. In order to estimate the free energy associated with the transition process, the work done by the applied stress is needed. To this end, we analyze the local strains from the HRTEM micrograph [45,46]. The strain distributions of the region immediately preceding the formation of wz-AlN are presented in the Supplementary. The average strain of each component ε_{xx}, ε_{xy}, and ε_{yy} is 2%, 1.6%,

and −7%, respectively. The TEM foil thickness is very thin (< 100 nm), much smaller compared to the other two dimensions, thus, it is reasonable to assume that there will be approximately no normal or shear stresses in the direction perpendicular to the film surface. Based this assumption, the strain component ε_{zz} is calculated to be ∼ 2.4%.

Here, we estimate the change in free energy associated with the nucleation of Shockley partial dislocations. The free energy per unit length along the z direction associated with the phase transformation from zinc blende to wurtzite can be written as:

$$E_{\text{free}} = E_{\text{interaction}} + E_{\text{self}} + \Delta E_{\text{cohesive}} + \Delta E_{\text{interface}} - W_{\text{applied\_stress}},$$

where the first term is the dislocation interaction energy; the second term is the dislocation self-energy; the third term is the cohesive energy difference between wurtzite and zinc blende phases of AlN, where the influence of the externally applied compressive strain has been considered; the fourth term is the interface energy difference; and the last term is the work done by the externally applied force. The resulting free energy associated with the phase transition and the individual contributors as a function of the width of the new phase (which is also the horizontal distance of the two Shockley dipoles) are plotted in Figure 5 (see Supplementary for details). The critical size of the wurtzite nucleus at the emergence of phase transformation can be estimated. The free energy of formation of wz-AlN reaches a maximum at the width of 0.7 nm and then decreases, indicating that the critical wz-AlN nucleus has to be wider than 0.7 nm in order to overcome the associated barrier. The width of the observed wz-AlN in our *in situ* indentation test is measured to be ∼ 1.3 nm, which agrees well with our calculated results.

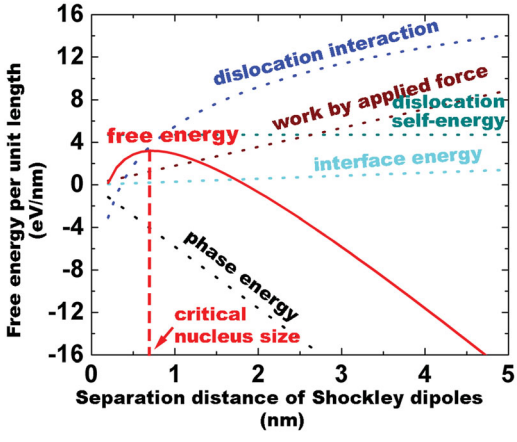

Figure 5. Plot of the free energy associated with the phase transition as a function of the width of the new phase. The critical size of the wurtzite nucleus is calculated to be ∼ 0.7 nm.

The attractive force between two Shockley dipoles as a function of the distance is calculated and plotted in the Supplementary. At the location of new phase generation, the resolved shear stress acting on the dipoles is measured to be ∼ 0.8 GPa, larger than their attractive interaction (0.6 GPa). Thus, the newly generated wz-AlN with the width of 1.3 nm is stable.

Following a similar process step, we analyze the local strains when the reversible phase transformation from wurtzite to zinc blende commences. Although the reversible phase transformation happens continuously during the loading process, the strain environment has changed significantly. As presented in the Supplementary, the average strain of each component ε_{xx}, ε_{xy}, and ε_{yy} decreases to 1.5%, 0.2%, and −3%, respectively. This is probably due to slight bending of the TEM foil when the indenter is pushed into the sample. With such strain condition, the local resolved shear stress decreases to 0.08 GPa, which is far less than the attractive force between two nucleated Shockley dipoles with a separation distance of 5.7 nm. Thus, the reverse phase transformation initiates through opposite-direction glide of the Shockley partials.

In summary, we demonstrated experimentally that the phase structure of synthesized AlN can be controlled through interface strains. In the as-deposited condition, metastable zb-AlN can be stabilized when Al thickness is less than 5 nm and AlN less than 1 nm. Via *in situ* high-resolution TEM straining experiments, we explored the phase transformation mechanism from zinc blende to wurtzite in AlN. We found the critical free energy barrier for this process to be ∼ 3.2 eV/nm and the critical size of wurtzite nucleus to be ∼ 0.7 nm wide. This reversible phase transformation mechanism is ascribed to the collective glide of Shockley partial dislocations on {111} planes of zb-AlN. The knowledge delivered from current work can be used to develop the instructive method of mechanically controlling the crystalline phase to either pure wurtzite or pure zinc blende or their combination in binary octet semiconductors to tailor the overall performance.

Acknowledgments

This work was performed, in part, at the Center for Integrated Nanotechnologies, an Office of Science User Facility operated for the U.S. DOE, Office of Science. Los Alamos National Laboratory, an affirmative action equal opportunity employer, is operated by Los Alamos National Security, LLC, for the National Nuclear Security Administration of the U.S. DOE under Contract No. DE-AC52-06NA25396.

Disclosure statement

No potential conflict of interest was reported by the authors.

Funding

This work was supported by the U.S. Department of Energy, Office of Science, Office of Basic Energy Sciences, and the Institute for Materials Science at Los Alamos National Laboratory. J.W. acknowledges financial support provided by the Nebraska Center for Energy Sciences Research (NCESR).

ORCID

Jian Wang http://orcid.org/0000-0001-5130-300X

References

[1] del Alamo JA. Nanometre-scale electronics with III–V compound semiconductors. Nature. 2011;479:317–323.
[2] Nan W, Niu Y, Qin H, et al. Crystal structure control of zinc-blende CdSe/CdS core/shell nanocrystals: synthesis and structure-dependent optical properties. J Am Chem Soc. 2012;134:19685–19693.
[3] Cui Y, Wei Q, Park H, et al. Nanowire nanosensors for highly sensitive and selective detection of biological and chemical species. Science. 2001;293:1289–1292.
[4] Yeh C-Y, Lu ZW, Froyen S, et al. Zinc-blende–wurtzite polytypism in semiconductors. Phys Rev B. 1992;46:10086–10097.
[5] Wang SQ, Ye HQ. A plane-wave pseudopotential study on III–V zinc-blende and wurtzite semiconductors under pressure. J Phys: Condens Matter. 2002;14:9579–9587.
[6] Assali S, Zardo I, Plissard S, et al. Direct band gap wurtzite gallium phosphide nanowires. Nano Lett. 2013;13:1559–1563.
[7] Patriarche G, Glas F, Tchernycheva M, et al. Wurtzite to zinc blende phase transition in GaAs nanowires induced by epitaxial burying. Nano Lett. 2008;8:1638–1643.
[8] Joyce HJ, Wong-Leung J, Gao Q, et al. Phase perfection in zinc blende and wurtzite III–V nanowires using basic growth parameters. Nano Lett. 2010;10:908–915.
[9] Johansson J, Karlsson LS, Svensson CP, et al. Structural properties of $< 111 >$ B -oriented III–V nanowires. Nature Mater. 2006;5:574–580.
[10] Glas F, Harmand JC, Patriarche G. Why does wurtzite form in nanowires of III–V zinc blende semiconductors? Phys Rev Lett. 2007;99:146101.
[11] McMahon MI, Nelmes RJ. Observation of a wurtzite form of gallium arsenide. Phys Rev Lett. 2005;95:215505.
[12] Caroff P, Dick KA, Johansson J, et al. Controlled polytypic and twin-plane superlattices in III–V nanowires. Nature Nanotech. 2009;4:50–55.
[13] Zheng H, Wang J, Huang JY, et al. Dynamic process of phase transition from wurtzite to zinc blende structure in InAs nanowires. Nano Lett. 2013;13:6023–6027.
[14] Li N, Yadav SK, Wang J, et al. Growth and stress-induced transformation of zinc blende AlN layers in Al-AlN-TiN multilayers. Sci Rep. 2015;5:18554.
[15] Perry PB, Rutz RF. The optical absorption edge of single-crystal AlN prepared by a close-spaced vapor process. Appl Phys Lett. 1978;33:319.
[16] Bourret A, Barski A, Rouvière JL, et al. Growth of aluminum nitride on (111) silicon: microstructure and interface structure. J Appl Phys. 1998;83:2003.
[17] Pérez Taborda JA, Caicedo JC, Grisales M, et al. Deposition pressure effect on chemical, morphological and optical properties of binary Al-nitrides. Opt Laser Technol. 2015;69:92–103.
[18] Yao SH, Su YL, Kao WH, et al. Tribology and oxidation behavior of TiN/AlN nano-multilayer films. Tribol Int. 2006;39:332–341.
[19] Mashimo T, Uchino M, Nakamura A, et al. Yield properties, phase transition, and equation of state of aluminum nitride (AlN) under shock compression up to 150 GPa. J Appl Phys. 1999;86:6710.
[20] Gorczyca I, Christensen NE, Perlin P, et al. High pressure phase transition in aluminium nitride. Solid State Commun. 1991;79:1033–1034.
[21] Madan A, Kim IW, Cheng SC, et al. Stabilization of cubic AlN in epitaxial AlN/TiN superlattices. Phys Rev Lett. 1997;78:1743–1700.
[22] Branicio PS, Kalia RK, Nakano A, et al. Shock-induced structural phase transition, plasticity, and brittle cracks in aluminum nitride ceramic. Phys Rev Lett. 2006;96:065502.
[23] Christensen NE, Gorczyca II. Optical and structural properties of III–V nitrides under pressure. Phys Rev B. 1994;50:4397–4415.
[24] Ching WY, Harmon BN. Electronic structure of AlN. Phys Rev B. 1986;34:5305–5308.
[25] Zoroddu A, Bernardini F, Ruggerone P, et al. First-principles prediction of structure, energetics, formation enthalpy, elastic constants, polarization, and piezoelectric constants of AlN, GaN, and InN: comparison of local and gradient-corrected density-functional theory. Phys Rev B. 2001;64:045208.
[26] Christensen NE, Gorczyca II. Calculated structural phase transitions of aluminum nitride under pressure. Phys Rev B. 1993;47:4307–4314.
[27] Siegel A, Parlinski K, Wdowik UD. Ab initio calculation of structural phase transitions in AlN crystal. Phys Rev B. 2006;74:104116.
[28] Xia Q, Xia H, Ruoff AL. Pressure-induced rocksalt phase of aluminum nitride: a metastable structure at ambient condition. J Appl Phys. 1993;73:8198–8200.
[29] Ueno M, Onodera A, Shimomura O, et al. X-ray observation of the structural phase transition of aluminum nitride under high pressure. Phys Rev B. 1992;45:10123–10126.
[30] Talwar DN, Sofranko D, Mooney C, et al. Elastic, structural, bonding, and defect properties of zinc-blende BN, AlN, GaN, InN and their alloys. Mater Sci Eng. 2002;90:269–277.
[31] Ramos LE, Furthmüller J, Leite JR, et al. Group-IV and group-V substitutional impurities in cubic group-III nitrides. Phys Rev B. 2003;68:085209.
[32] Dietl T, Ohno H, Matsukura F, et al. Zener model description of ferromagnetism in zinc-blende magnetic semiconductors. Science. 2000;287:1019–1022.
[33] Taniyasu Y, Kasu M, Makimoto T. An aluminium nitride light-emitting diode with a wavelength of 210 nanometres. Nature. 2006;441:325–328.

[34] Petrov I, Mojab E, Powell RC, et al. Synthesis of metastable epitaxial zinc-blende-structure AlN by solid-state reaction. Appl Phys Lett. 1992;60:2491–2493.
[35] Kim IW, Madan A, Guruz MW, et al. Stabilization of zinc-blende cubic AlN in AlN/W superlattices. J Vac Sci Technol A. 2001;19:2069–2073.
[36] Cai D, Kang J.: Phase transition of ultrathin AlN interlayer at AlGaN/GaN interface. Appl Phys Lett. 2007;90:121909.
[37] Liu Y, Chen Y, Yu KY, et al. Stacking fault and partial dislocation dominated strengthening mechanisms in highly textured Cu/Co multilayers. Int J Plast. 2013;49:152–163.
[38] Ham B, Zhang X. High strength Mg/Nb nanolayer composites. Mater Sci Eng: A. 2011;528:2028–2033.
[39] Chen Y, Liu Y, Sun C, et al. Microstructure and strengthening mechanisms in Cu/Fe multilayers. Acta Mater. 2012;60:6312–6321.
[40] Yadav SK, Wang J, Liu XY. Ab initio modeling of zincblende AlN layer in Al-AlN-TiN multilayers. J Appl Phys. 2016;119:224304.
[41] Wang J, Anderoglu O, Hirth JP, et al. Dislocation structures of Σ3 {112} twin boundaries in face centered cubic metals. Appl Phys Lett. 2009;95:021908.
[42] Wang J, Beyerlein IJ, Tomé CN. An atomic and probabilistic perspective on twin nucleation in Mg. Scripta Mater. 2010;63:741–746.
[43] Liu L, Wang J, Gong SK, et al. High resolution transmission electron microscope observation of zero-strain deformation twinning mechanisms in Ag. Phys Rev Lett. 2011;106:175504.
[44] Hirth J, Lothe J. Theory of dislocations. New York (NY): Wiley; 1982.
[45] Li N, Yadav SK, Liu XY, et al. Quantification of dislocation nucleation stress in TiN through high-resolution *in situ* indentation experiments and first principles calculations. Sci Rep. 2015;5:15813.
[46] Li N, Misra A, Shao S, et al. Experimental quantification of resolved shear stresses for dislocation motion in TiN. Nano Lett. 2015;15:4434–4439.